Title of Publication *Edited by*
TMS (The Minerals, Metals & Materials Society), Year

PHASE TRANSFORMATIONS DURING SERVICE AGING OF NICKEL BASED SUPERALLOY PYROMET 31V

Neal D. Evans, Philip J. Maziasz and John J. Truhan

Metals & Ceramics Division, Oak Ridge National Laboratory
P.O. Box 2008, Oak Ridge, TN 37831-6376 USA

Keywords: Nickel-base Superalloy, Precipitation, Electron Diffraction, Analytical Electron Microscopy

Abstract

The general high-temperature and performance limitations of various critical exhaust components (e.g., exhaust valve, exhaust manifold, turbocharger housing) used in advanced natural gas reciprocating engine systems (ARES) are being investigated. These baseline data will then be used to identify cost-effective materials with greater temperature capability and performance for such components. In this study, exhaust valves manufactured from wrought Ni-based superalloy Pyromet 31V have been examined in both the as-manufactured (fresh) and engine-tested (2400 h of service) condition to discern the effects of long term engine exposure. Service temperatures were estimated for the various valves at 650 – 700°C. In the as-manufactured condition, the base material of the valve can be described as having a γ matrix that is strengthened by γ' precipitates, with $M_{23}C_6$ carbides residing along grain boundaries and MC carbides present within the austenite. After service aging, the alloy is marked by coarsened γ', increased $M_{23}C_6$ carbide precipitation in grain boundaries, MC carbides, and the precipitation of α-chromium laths within the austenite grains.

Introduction

Next generation natural gas reciprocating engines will have higher in-cylinder pressures and temperatures in order to meet the goals of higher power density and efficiency, and lower emissions. A program to address the general high-temperature, performance, and tribology limitations of various critical exhaust components (e.g., exhaust valve, seats, exhaust manifold, turbocharger housing) for advanced natural gas reciprocating engine systems (ARES) has focused on the use of Ni-based superalloys in exhaust valves for higher temperature operation. These valves are complex systems, with weld-overlays on the valve seat, and coatings on the combustion face. The fillet region of the exhaust valve can see temperatures close to 700°C, and temperatures for valves within advanced ARES engines may be even higher. Candidate materials for these components face the challenging goals of having increased life and reliability under increased service temperature and pressure, while abiding within the constraint of reasonable cost.

In collaboration with ARES OEM's and their component suppliers, Oak Ridge National Laboratory (ORNL) is characterizing the effects of long term engine exposure on intake and exhaust valves, their seats, and other exhaust components. With an appropriate baseline developed for mechanical and oxidation behavior of current materials and components, along with underlying knowledge of service-related microstructural changes in various alloys, candidate materials and processing options for next generation components can be identified.

Experimental Procedures

Both as-manufactured (alloy in fresh condition is solutionized, and heat treated to precipitate γ') and engine-tested valve exhaust valves of Pyromet 31V (Ni-22Cr-15Fe alloy with Ti and Al additions for γ' precipitation hardening) were used to obtain specimens for electron microscopy. Specimens were obtained from the fillet region of the valve. This is the region subject to the greatest operating temperatures and tensile stresses, and for the valves examined, is located approximately 25 mm behind the valve combustion face. Scanning electron microscopy (SEM) and transmission electron microscopy (TEM) were performed with a JEOL 6500F SEM, a Philips XL30FEG SEM, and a FEI Tecnai20 TEM. Additionally, some electron energy-loss spectrometry (EELS) was performed in the scanning-transmission mode of a Philips CM200FEG TEM. The SEM was performed on mechanically polished and unetched metallographic specimens. The SEM images were acquired at 15 kV with either the secondary electron (SE) or the backscattered electron (BSE) detector. Phase identification, and quantification (Emispec Vision) of major elements (for Z >10) present in phases observed in the SEM was accomplished with energy dispersive X-ray spectrometry (EDS). All EDS was conducted at 15 kV to ensure sufficient overvoltage for the NiKα excitation. The TEM was performed at 200 kV on conventionally prepared electropolished disks. The EDS acquisition in the TEM was performed in the nanoprobe mode with electron probes ~50 nm diameter (FWHM). Phase identification was accomplished from EDS and EELS measurements, and the analysis of selected area diffraction (SAD) patterns.

Experimental Results

Backscattered electron SEM images of the wrought alloy in the as-manufactured condition are show in Figure 1. In this condition, the alloy has an equiaxed microstructure of typically 50 – 100 μm diameter grains (Fig. 1a); annealing twins are common as are intragranular carbides. At higher magnification (Fig. 1b), a fine precipitate phase can be seen within some grain boundaries. The atomic number (or Z) contrast mechanism that produces the BSE images infers

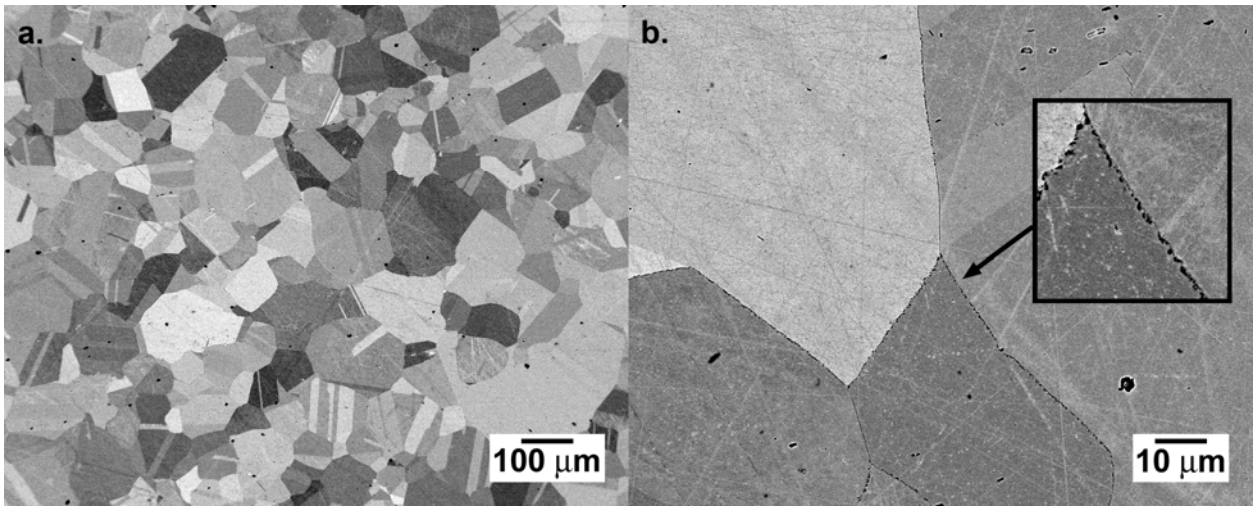

Figure 1 Backscattered SEM images of wrought base alloy in exhaust valve prior to service. a.) austenite grains have typically 50 - 100 μm diameters; b.) grain boundaries are decorated with small precipitates, while grain interiors contain MC carbides.

that some intragranular precipitates have a higher average Z than the austenite grains, whereas some, appearing dark in the figure, have a lower average Z than the austenite. EDS spectra

acquired from these two types of precipitates indicated the high-Z and low-Z phases are enriched in Nb and Ti, respectively. These, therefore, appear to be NbC and TiC MC-type carbides.

When examined in the TEM, the matrix was found to consist of face centered cubic (fcc) γ, with dispersed γ'. Selected area diffraction patterns, such as that shown in Figure 2a, show the superlattice reflections from γ' superimposed on those from the γ matrix. The morphology and size of the γ' phase is revealed in the dark-field image of Figure 2b, which was acquired at g = $(100)_{\gamma'}$. Here, the spherical γ' has an average diameter of 48 nm.

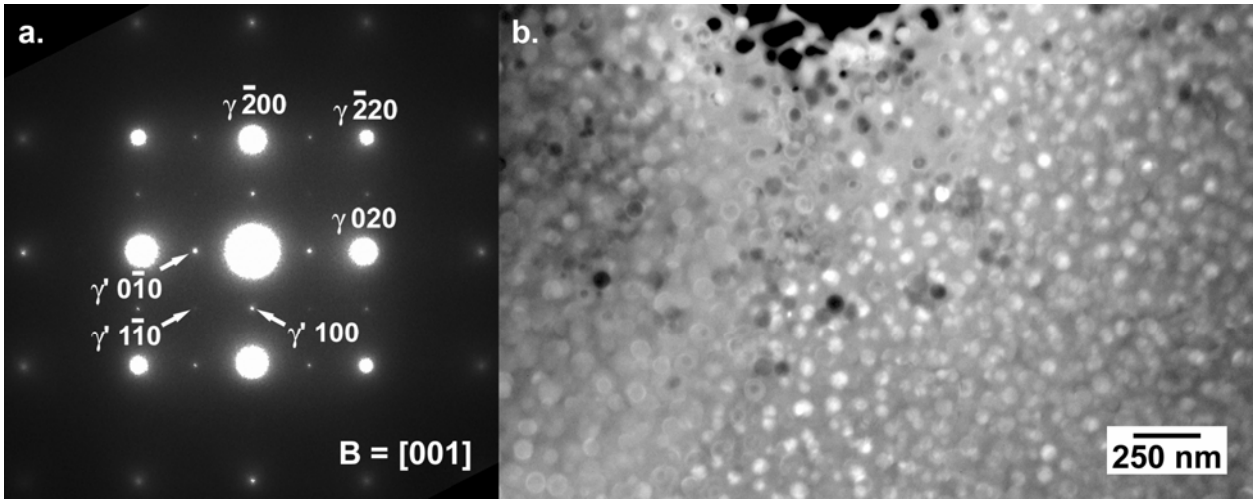

Figure 2 a.) SAD pattern from γ matrix, showing γ' superlattice reflections, B = [001]; b.) centered dark-field image of γ matrix using $(100)_{\gamma'}$ reveals the size of the γ ' precipitates.

The grain boundary precipitates in the as-manufactured alloy, noted in Figure 1b, were examined in the TEM (Figure 3). These precipitates are typically 200 nm in size. Selected area diffraction patterns were acquired from the precipitate arrowed in Figure 3a, and were indexed as being from fcc $M_{23}C_6$, as shown in the [011] pattern of Figure 3b. The value for the lattice parameter a_0, determined from indexed diffraction patterns, was 1.065 nm, and is in excellent agreement with reported values for that phase [1,2]. In the TEM, EDS spectra were obtained from this precipitate, as well as other precipitates along the grain boundary and quantified using a

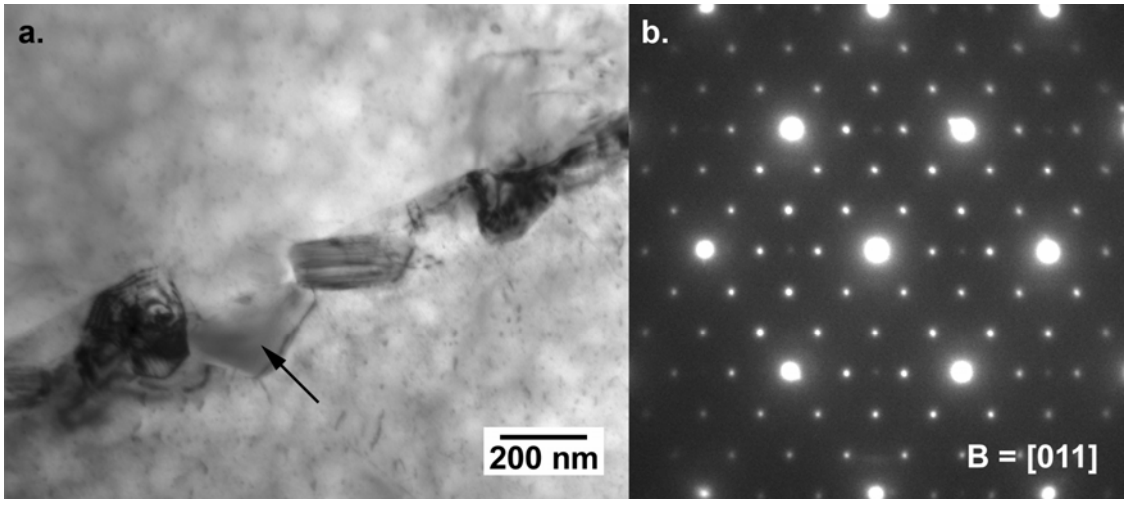

Figure 3 a.) Precipitates decorate grain boundaries in the fresh alloy prior to service; b.) SAD pattern from grain boundary precipitate arrowed in the bright-field image indicates precipitate is $M_{23}C_6$ carbide.

standardless thin-film approximation. The resulting measure of composition for these grain boundary precipitates for Z >10 is Cr-6.9Mo-5.1Ni-2.5Fe-0.2Ti (wt%), which is also consistent with these being $M_{23}C_6$ carbide. No other phases were observed in grain boundaries of the base alloy in the as-manufactured condition.

Significant changes occurred in the microstructure of the base alloy during service aging 2400 h at 700°C. As shown in Figure 4, the grain size did not coarsened during service (Figure 4a), but grain boundaries are now heavily decorated with a precipitate phase, and another phase having a lath morphology has precipitated within grain interiors (Figure 4b). The NbC and TiC carbides are readily observed as light and dark intragranular precipitates, respectively, in Figure 4b.

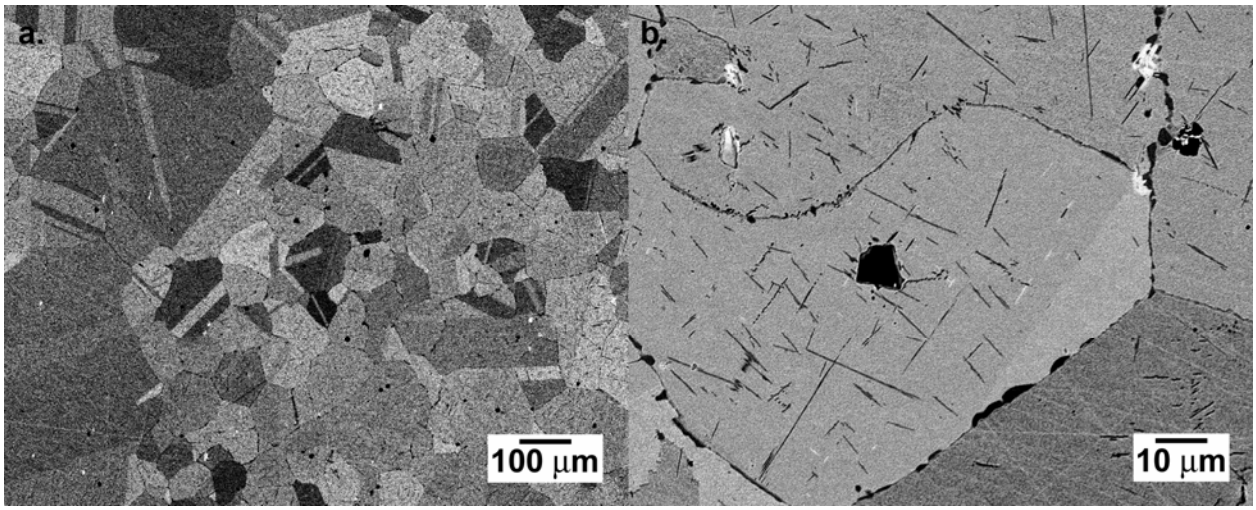

Figure 4 Backscattered SEM image of wrought base alloy in an exhaust valve following 2400 h service at 700°C. a.) grain size has not coarsened during service; b.) grain boundaries are heavily decorated with precipitates, and a lath phase has precipitated in grain interiors.

Service aged valve material was also examined in the TEM. The morphology and size of the γ' is revealed in dark-field images, g = $(100)_{\gamma'}$ (Figure 5). Here, the γ' has maintained its spherical morphology, although its average diameter varies with service temperature: 158 and 171 nm with 2400 h service at 650°C (Figure 5a) and 700°C (Figure 5b), respectively.

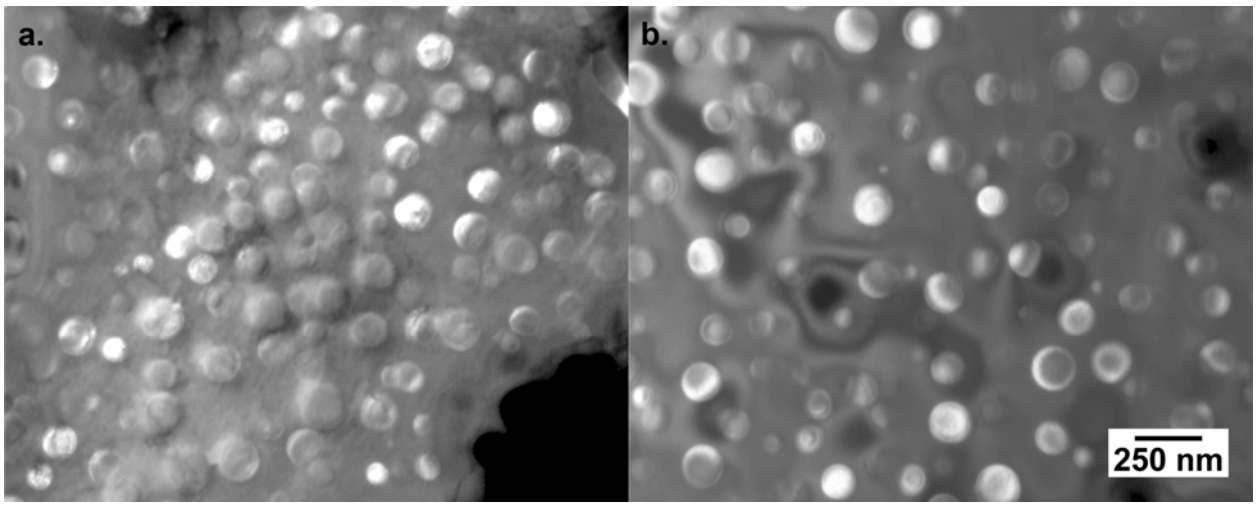

Figure 5 Centered Darkfield images of γ matrix after service aging a.) 2400 h at 650°C, and b.) 2400 h at 700°C.

As shown in Figure 6, the $M_{23}C_6$ grain boundary precipitates which were typically 200 nm in size have coarsened during service aging to typically 300 – 500 nm in size. The precipitate arrowed in Figure 6a, was used to obtain the SAD pattern presented in Figure 6b. This can be indexed as coming from a [011] zone in $M_{23}C_6$ carbide. EDS spectra were acquired from each precipitate noted along this grain boundary. All spectra display similar relative amounts of constituents corresponding to $M_{23}C_6$ carbide. No other phases were observed in the grain boundaries.

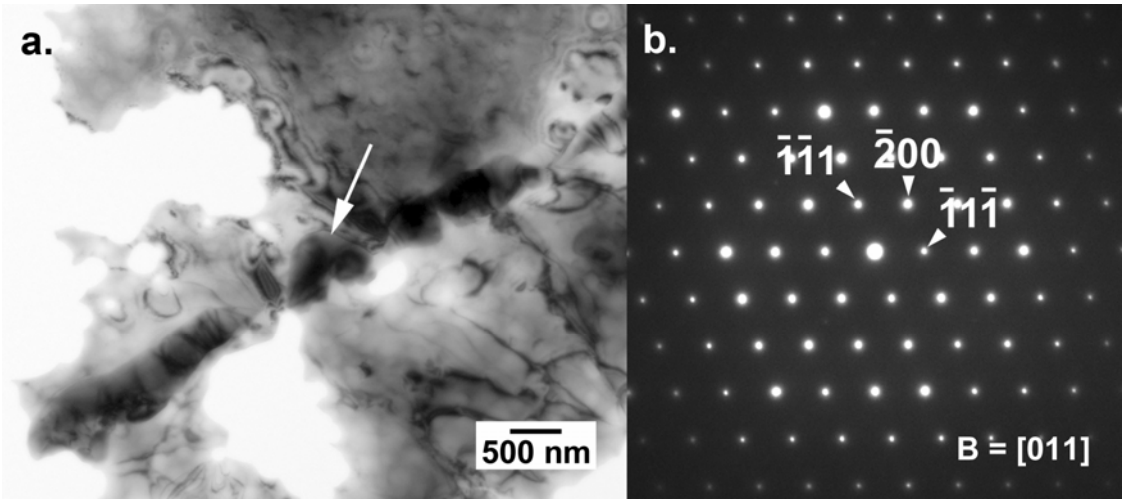

Figure 6 a.) Coarsened precipitates decorate grain boundaries in the wrought alloy following service aging; b.) SAD pattern from grain boundary precipitate arrowed in the bright-field image indicates precipitate is $M_{23}C_6$ carbide.

The phase having a lath morphology, which precipitated during service aging, was also examined in the TEM (Figure 7a). The composition of these laths was measured by EDS as being 93.9Cr–3Mo–2.1Fe–1Ni (wt%). Selected area diffraction patterns, acquired from the region of the lath indicated in Figure 7a, are presented as Figures 7b, 7c, and 7d. These can be indexed as [001], [111], and [113] zones, respectively, for body centered cubic (bcc) α-Cr. The value of a_0 measured in these diffraction patterns is 0.2883 nm, and agrees quite well with the established value of 0.28839 nm [3].

To verify that the lath phase was not an unidentified carbide, nitride, or oxide, the amount of, if present, carbon, nitrogen, and oxygen, associated with these laths was determined from electron energy-loss spectrometry. Spectra were acquired from these and other features of the microstructure, and are presented in Figure 8. Although the expected constituents are observed for the γ and γ' phases, and only chromium is noted in the spectrum from the lath, no significant carbon (C K onset at 286 eV), nitrogen (N K onset at 401 eV), or oxygen (O K onset at 532 eV) are present in any phase examined. These EELS results support and confirm the diffraction experiments which indicate the lath phase is α-Cr.

Phase equilibria anticipated for the base wrought alloy composition were calculated using the materials properties modeling program JMatPro 2.2 from Sente Software, UK [4]. The associated materials properties database referenced by JMatPro to predict phase stability was Ni-DATA [5]. The phase fields predicted and their ranges are presented in Figure 9 where there is good agreement between the phases observed and those predicted. Additionally, the composition of the α-Cr phase at 650^{o}C predicted by JMatPro is 93Cr–1.8Mo–4.7Fe–0.5Ni (wt%) with trace amounts of the remaining constituents. This also agrees well with the composition measured by EDS.

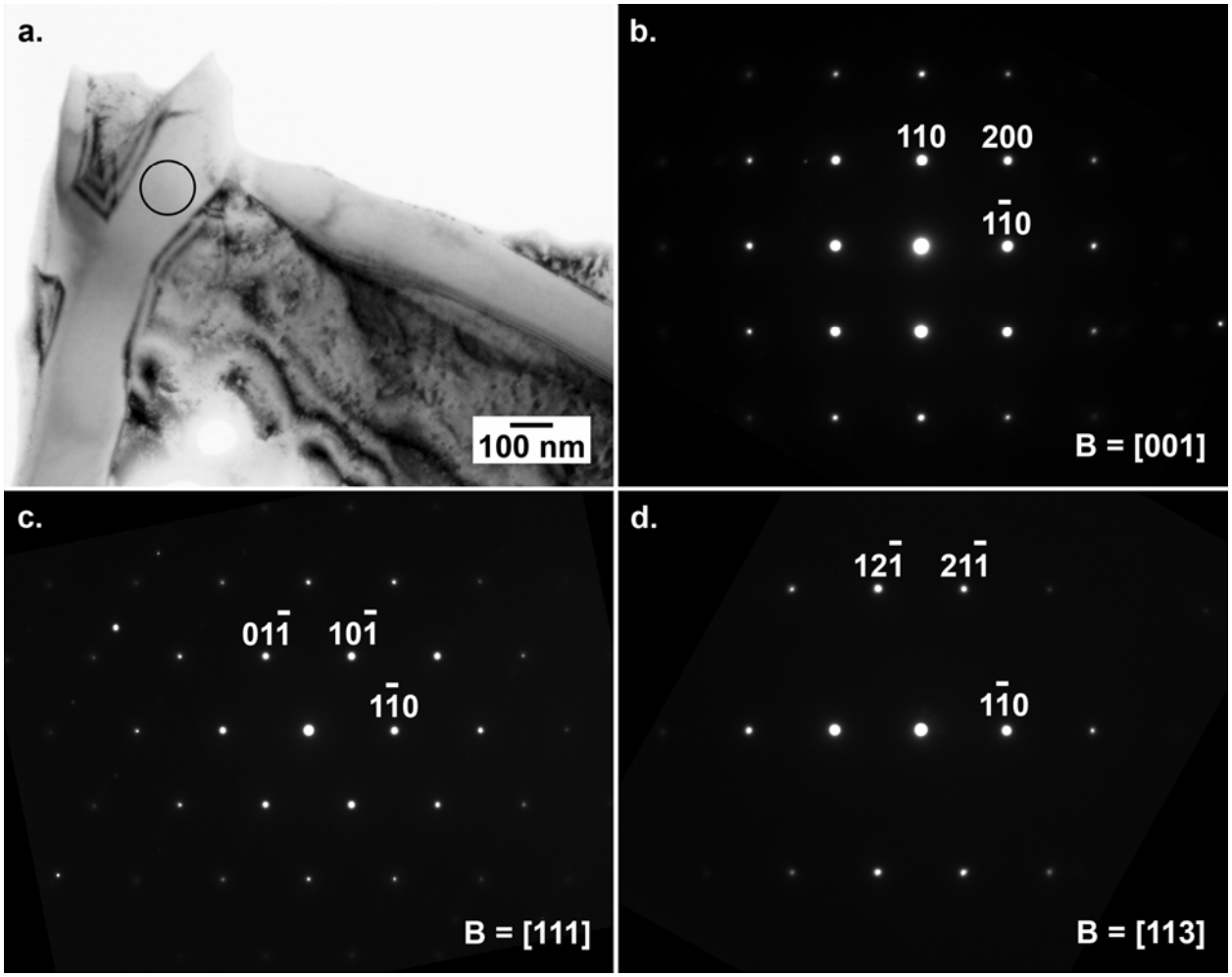

Figure 7 a.) TEM image of lath phase developed during service aging of wrought base alloy. The SAD patterns obtained from the lath phase are indexed as bcc α-Cr at b.) [001]; c.) [111]; d.) [113]

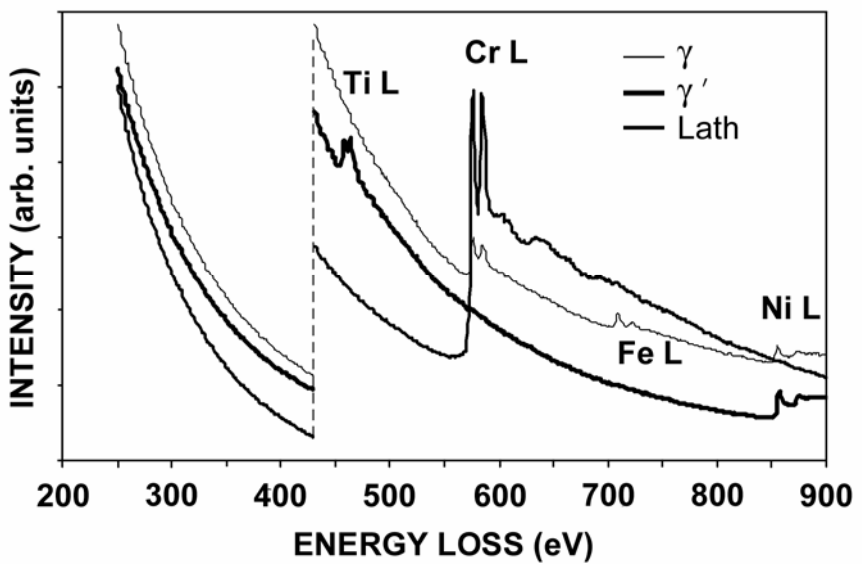

Figure 8 Electron energy-loss spectra reveal neither carbon, nitrogen, nor oxygen are present in the lath phase

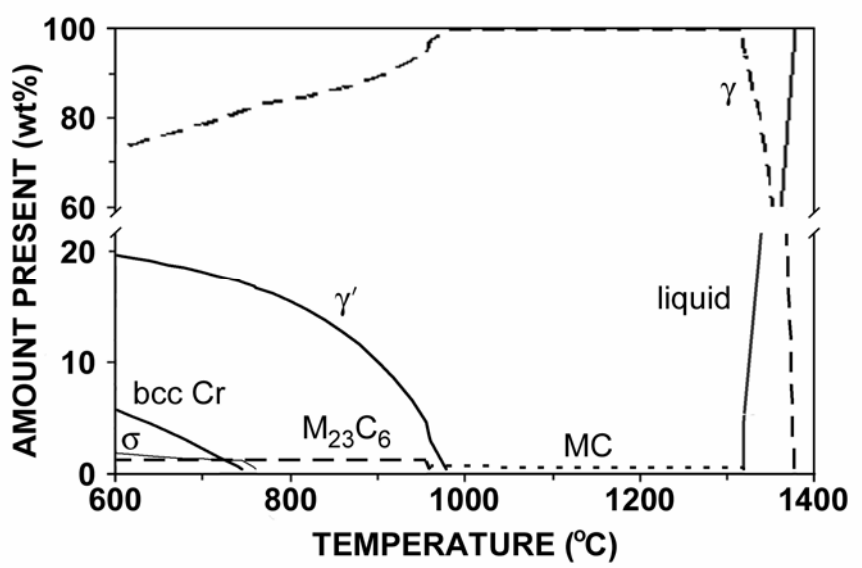

Figure 9 Phase equilibria were calculated using nominal composition for the base alloy

Discussion

Finely dispersed γ' precipitates strengthen the grains of new exhaust valves, particularly at high temperatures. As expected, however, this γ' coarsens during service, which reduces strength. Additionally, service at higher temperatures accelerates this coarsening. The grain size of the austenite did not significantly coarsen during service aging. This is likely due to the boundaries being stabilized by the $M_{23}C_6$ precipitates, which remained stable during service. Overall, after 2400 h service at 700°C, the base alloy is showing significant effects of aging, and is beginning to show changes in microstructure that could contribute to degradation and failure after much longer service. For operation at higher temperatures and stresses, these exhaust valves may have limits based on stability of the original microstructure, and understanding these limitations helps with the selection of an alternative alloy.

Direct observation of α-Cr precipitation in a superalloy is somewhat unusual and seldom mentioned [6], it has been observed in Inconel 718 alloys. Following annealing alloy 718 for 747 h at 648.9°C (1200°F), Barker et al. designated extra peaks in X-ray diffraction results as a bcc "alpha prime," and tabulated d-spacings for this phase which correspond to α-Cr [7]. The precipitation of α-Cr in 718 has been reported following long exposure time in the temperature range 539 - 704°C, where its extent was seen to increase with exposure time [8]. Additionally, α-Cr has been identified as a precipitate phase in the aluminide coating matrix of a nickel-base superalloy [9]. It is unclear what effect the α-Cr laths have on the mechanical properties of the alloy, but they do signal the fact that the chromium content of the alloy is above the solubility limit at the aging conditions. It may be this phase offers no deleterious effect on the alloy. However, the potential for embrittlement exists if oxygen is allowed to react with the α-Cr to form Cr_2O_3.

Interestingly, the only other phase predicted by JMatPro to form, but not observed in this base alloy following service aging, is the topologically close-packed (tcp) phase σ. This body-centered tetragonal phase forms after extended exposure in the range 540 - 980°C [6]. The absence of σ in this alloy may be due to insufficient kinetics, or limitations in the thermodynamic database. However, σ requires significant amounts of chromium and iron to form, and during service aging of this alloy, both the growth and additional precipitation of

$M_{23}C_6$ at grain boundaries and the precipitation of α-Cr laths may consume the excess Cr before the σ can form. The retardation of σ in a superalloy due to formation of $M_{23}C_6$ has been observed elsewhere [10].

Conclusions

The microstructure of the wrought and heat-treated superalloy used for exhaust valves of a natural gas reciprocating engine system has been determined in both the as-manufactured condition, and following 2400 h of actual service. In the as-manufactured condition, the γ matrix is strengthened by a fine dispersion of γ', and grain boundaries are stabilized by $M_{23}C_6$ carbides. During service, the microstructure undergoes transformations which likely degrade the mechanical properties of the alloy, including γ' coarsening, increased $M_{23}C_6$ carbide precipitation in grain boundaries, and precipitation of α-Cr within the grains.

Acknowledgments

Research supported (NDE, PJM, JJT) by the Assistant Secretary for Energy Efficiency and Renewable Energy, Office of Distributed Energy and Electrical Reliability, and (ORNL SHaRE User Facility) by the Division of Materials Sciences and Engineering, Office of Basic Energy Sciences, U.S. Department of Energy, under contract DE-AC05-00OR22725 with UT-Battelle, LLC.

References

1. A.L. Bowman, G.P. Arnold, E.K. Storms, and N.G. Nereson, "The Crystal Structure of $Cr_{23}C_6$," Acta Cryst. B **28**, (1972) 3102-3103.
2. K.W. Andrews, D.J. Dyson, and S.R. Keown, *Interpretation of Electron Diffraction Patterns* (New York, NY: Plenum Press, 2nd ed., 1971), 202.
3. Selected Powder Diffraction Data for Metals and Alloys, 1st ed., Volume 1, #6-694, International Centre for Diffraction Data, 1978.
4. N. Saunders, X. Li, P. Miodownik and J. Ph. Schillé in *Materials Design Approaches and Experiences*, ed. J-C. Shao et al, (Warrendale, PA, TMS, 2001), p 185-197.
5. N. Saunders, M. Fahrmann and C. J. Small, in *Superalloys 2000U*, ed. K.A. Green, T.M. Pollock and R.D. Kissinger, (Warrendale, PA, TMS, 2000), 803.
6. M.J. Donachie and S. Donachie, *Superalloys: A Technical Guide* (Materials Park, OH: ASM Intl., Pub., 2002), 28.
7. J.F. Barker, E.W. Ross, and J.F. Radavich, "Long Time Stability of Inconel 718" *Journal of Metals*, Janury 1970 31-41.
8. J.F. Radavich, "Effect of Alpha Chromium on Long Time Behavior of Alloy 718," *Superalloys 718, 625, 706 and Various Derivatives* (Pittsburgh, PA: The Minerals, Metals & Materials Society, 1997), 409-415.
9. W.F. Gale and J.E. King, "Precipitation of Chromium Containing Phases in Aluminide Coated Nickel-base Superalloy Single Crystals," *J. Mat. Sci* **28**, (1993) 4347-4354.
10. Q.Z. Chen and D.M. Knowles, "Retardation of σ-Phase Transformation in Modified Superalloy RR2072" *Metall. Trans. A*, 33 (2002), 1319–1330.